

High-resolution mapping of mainland China's urban floor area



Miao Liu^a, Jun Ma^b, Rui Zhou^c, Chunlin Li^{a*}, Dikang Li^a, Yuanman Hu^a

^a CAS Key Laboratory of Forest Ecology and Management, Institute of Applied Ecology, Chinese Academy of Sciences, Shenyang 110016, China

^b Ministry of Education Key Laboratory for Biodiversity Science and Ecological Engineering, Coastal Ecosystems Research Station of the Yangtze River Estuary, Institute of Biodiversity Science, School of Life Sciences, Fudan University, Shanghai 200438, China

^c School of Environmental and Geographical Sciences, Shanghai Normal University, Shanghai 200234, China

HIGHLIGHTS

- A new approach was developed to map urban floor area from nighttime lights data.
- The first urban floor area map in mainland China.
- The coastal area of mainland China have the highest value and intensity of urban floor area.

ARTICLE INFO

Keywords:

Floor area map
LUOJIA 1-01 NTL images
Random forest
Mainland China

ABSTRACT

Urbanization studies are of global interest and mainly focus on mapping urban areas and areas of expansion using remote sensing data. However, information about the 3-dimensional characteristics or expansion of urban buildings is absent due to difficulties in data acquisition. Quantifying the urban floor area is crucial for assessing urban 3-D morphology. We used a random forest regression model to predict the first urban floor area of mainland China at a 130-m spatial resolution based on high spatial resolution nighttime light LUOJIA 1-01 images (130-m), a population map (100-m), and a single building dataset encompassing 71 cities. The predicted floor area (PFA) map for mainland China was estimated from the single building dataset of 50 cities, and data from the other 21 cities were used to estimate the accuracy. The results showed that the total accuracy of the PFA map is strong ($R^2 = 0.68$, RMSE = 7277.46 m²/ha). The PFA map overestimated the values in low value areas and underestimated the values in high value areas. The accuracy was also acceptable at the single city scale based on the results from six cities ($R^2 > 0.6$). The calculated floor area map for 71 cities was merged with the PFA map by replacing the values in the corresponding locations to generate the final predicted floor area (FPFA) map, which enabled higher accuracy. The total floor area is 76038.39 km², which is 0.79% of the total area of China. The general distribution of the floor area amount and intensity showed that the coastline had a higher intensity than the inner region of the country and the southern region had a higher intensity than the northern urban area along the coastline. The floor area distribution was extremely uneven among the provinces. The top six provinces represent 50.01% of the total floor area; however, the last six provinces represent only 3.31%. The high spatial resolution FPFA map of mainland China calculated by us has great potential application in urban ecology research, such as the impact of FPFA on heat island and haze.

1. Introduction

Urbanization is a comprehensive phenomenon that simultaneously involves changes in demographics, economic conditions and land cover, which are characterized by the increases in impervious surfaces, building stocks and transportation infrastructure (Zhang and Seto, 2011). Urban land covers represents only a small proportion of the global

terrestrial surface, but is home to more than half of the world's population (Flörke et al., 2018). A total of 55% of the world's population lived in urban areas in 2018, and 68% of the world's population is projected to live in urban areas by 2050 (UN, 2018). China has the greatest population and has experienced unprecedented and rapid urbanization over the last several decades (Seto et al., 2000). Due to land resources limitations, rapid urbanization causes urban expansion in 2-

* Corresponding author.

E-mail address: Lichunlin@iae.ac.cn (C. Li).

(2-D) and 3- (3-D) dimensions, especially in China (Cao et al., 2021). The 3D urban expansion results in more high buildings and increased floor area amount/intensity.

Many studies of the changes in urban land use/cover have been carried out using remote sensing (RS) technology (Ge et al., 2019; Liu et al., 2020). Most urban studies using RS focus on the surface status, using projected and 2-D information. The sources of data for urban studies include RS images, including Landsat TM/ETM images (Gong et al., 2013), the Defense Meteorological Satellite Program's Operational Linescan System data (DMSP/OLS) (L. Imhoff et al., 1997) and Modis images (Liu et al., 2015), which exist at global or national scales. In a single city or a smaller study area, optical high spatial resolution RS images are the main sources of data and include SPOT5, Quickbird, IKONOS, and Sentinel images (Leinenkugel et al., 2011; Sawaya et al., 2003). As the built-up area expanded, urban buildings were increasingly reconstructed inside of Chinese cities (Xu et al., 2019). China had 661 cities in 2018; all of these cities were partly reconstructed over the last several decades (Statistics, 2018). Several case studies have attempted to analyze the change in the urban 3-D surface (Kedron et al., 2019; Liu et al., 2017) and its relationship with urban environmental conditions (Alavipanah et al., 2018; Zheng et al., 2019). The ideal source of data for urban 3-D change is a single urban buildings data feature, which is difficult to obtain for a large study area. Except for the single urban buildings source of data from a construction administrator department or an electronic navigator, RS sources of data are powerful technologies used to extract information about urban buildings, such as aerial images (Suveg and Vosselman, 2002), high-resolution satellite imagery (Khosravi et al., 2014), Light Detection And Ranging (LIDAR) data (Zhao et al., 2020), and synthetic aperture radar (SAR) images (Ok, 2013). At present, the LIDAR and SAR data are the most powerful tools for extracting information about urban buildings (Niemeyer et al., 2014; Schunert and Soergel, 2012). However, the data is limited due to few archive data and high prices. Therefore, information about national and global urban 3-D buildings is very difficult to extract and is urgently required.

The nighttime light (NTL) data, represented by the Defense Meteorological Satellite Program's Operational Linescan System (DMSP/OLS) and the Visible/Infrared Imager/Radiometer Suite (VIIRS/DNB) (Miller et al., 2012), do not reflect urban land use or built-up areas, but the images are related to many characteristics of urban settlements and the common human activities that occur in urban areas. NTL indicated the intensity of urban human activities, which is closely related to the types of urban functional areas and the floor area ratio. NTL data has been widely used in urban studies (Li and Zhou, 2017), including studies on urban areas (Hu et al., 2020), urban impervious surfaces (Ma et al., 2014), population density (Lo, 2001; Ye et al., 2019), built-up area maps (Ma et al., 2012), carbon emission estimations (Doll et al., 2000), and electric power consumption (Amaral et al., 2005). And Li et al. (2020) showed that NTL data combined with other spatial data could accurately estimate building height in large scale (Li et al., 2020). In recent years, several new NTL satellites with high resolution images were launched, including CUMULOS, Aerocene 5, Jilin-1, and EROS-B. However, the new images were not applicable (Levin et al., 2020). The LUOJIA is a new NTL monitoring satellite series, which includes 3 satellites. LUOJIA 1-01 was launched in June 2018 by China (Li et al., 2018), the other two satellites are planned to launch before 2022. The spatial resolution of the LUOJIA 1-01 TNL production is 130 m, which provides images of much higher spatial resolution than DMSP/OLS (3000 m) and VIIRS/DNB (740 m). The image of China in 2018 was published in January 2019. The LUOJIA 1-01 can provide an image of the whole planet in 15 days in ideal conditions. The high spatial resolution LUOJIA NTL images provide powerful data for urban settlement information extraction at the national or global scales. New high-resolution nighttime light (NTL) images provide possibility for 3-D urban studies at large scale in near real-time.

The NTL data can be oversaturated in urban areas, especially urban cores, which limits the accuracy of NTL data application in urban areas.

Table 1
Datasets used in floor area mapping.

Dataset	Time	Spatial resolution	Source
Single building dataset in 71 cities	2017	Each building with stories data	Baidu Map Services, China; Bureau of Surveying and Mapping
LUOJIA 1-01 nighttime lights imagery	2018	130 × 130 m	High resolution earth observation system Hubei data and application network (http://www.hbeos.org.cn/)
Population Mainland China dataset	2017	100 × 100 m	Chinese Population map (Ye et al., 2019).
Global urban area map	2015	30 × 30 m	Global urban area map (Liu et al., 2018).
NDVI from Landsat	2018	30 × 30 m	

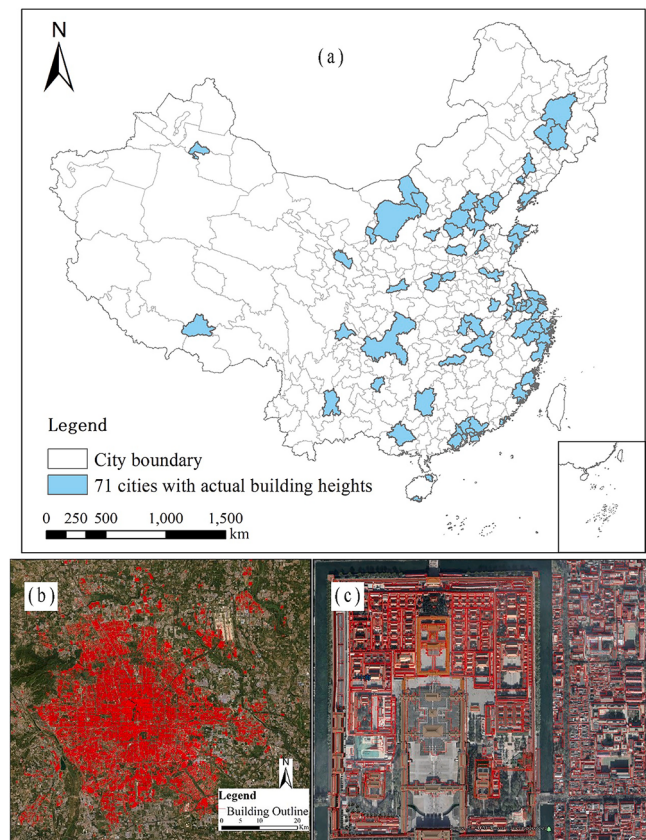


Fig. 1. The actual building feature dataset. (a) The 71 cities with actual building heights; (b) The buildings outline of Beijing; (c) Imperial Palace of Beijing and surrounding area.

The adjusted NTL Urban Index (VANUI), which combines Normalized Difference Vegetation Index (NDVI) with NTL, was proposed to reflect the biophysical and urban characteristics with greater accuracy, which can significantly reduce the NTL saturation and increases the variation in the data (Zhang et al., 2013). Assessments of its application in areas of urban impervious surfaces, urban expansion and electric power consumption have proved the effectiveness of this method (Ge et al., 2019; Li et al., 2019; Ma et al., 2014).

The primary objectives of this study were to: (1) develop a method to map the 3-D building information, represent the floor area, and develop the first urban floor area of mainland China; (2) analyze the spatial distribution of the floor area in China; and (3) discuss the potential implications of the floor area map and LUOJIA 1-01 NTL images.

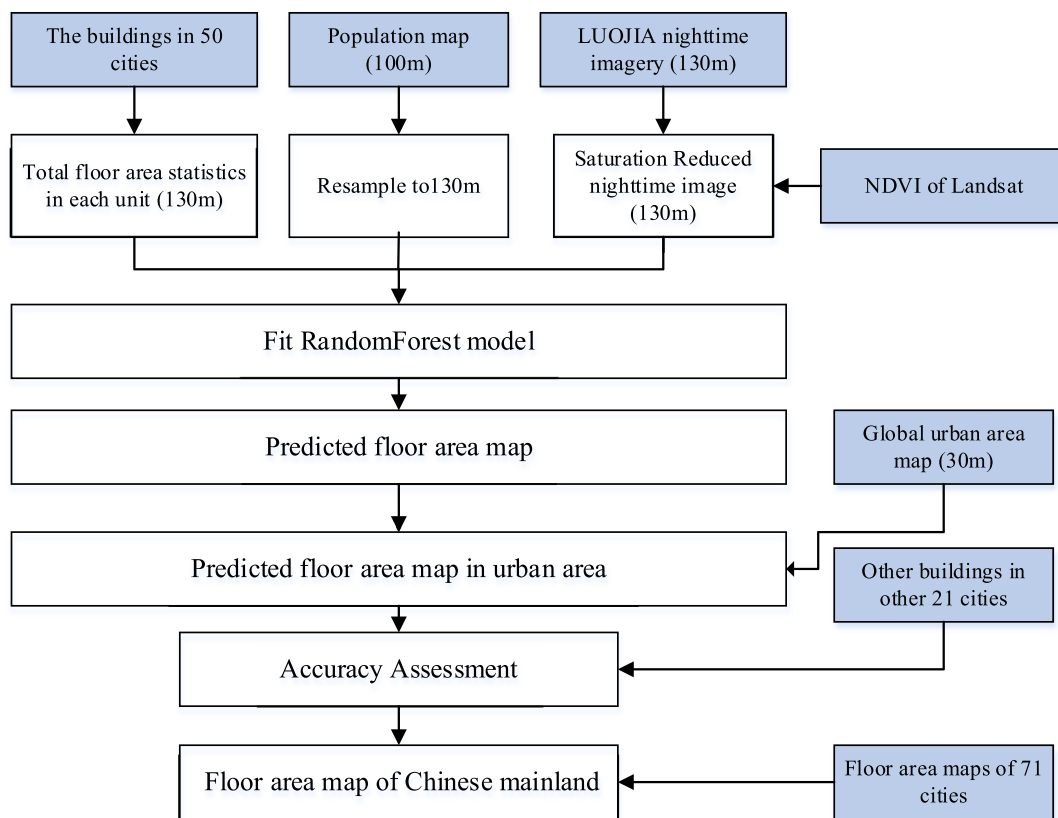


Fig. 2. Flowchart for the floor area mapping and assessment.

2. Data and preprocessing

Table 1 lists five types of data that were used to map the floor area and were used in the accuracy assessment of the results.

2.1. Building feature dataset

The single building polygon feature dataset for 71 cities in China was collected from Baidu Map (www.map.baidu.com/). The dataset includes all the metropolises (Beijing, Shanghai, Guangzhou, Shenzhen, and Tianjin et al.) and all the capitals of provinces (Fig. 1(a)). The dataset includes each single building with story information about the core part of the built-up area, such as in Beijing, Shanghai, Shenyang, and Panjin, when this information included 323769, 574250, 174,417 and 68,091 single buildings, respectively. Fig. 1(b and c) shows that the outline of the buildings perfectly matches the actual buildings based on the high spatial resolution google earth images. The actual heights of the 519 different buildings in Shenyang city were measured in 2018 using a LaserCraft Contour XLRic for estimating the accuracy of building heights dataset. The overall mean height deviation of this dataset was 1.02 m, and the accuracy was 86.78%.

The floor area was calculated using a projected area and the story number of the building. The fishnet feature map was generated with 130-m size of each polygon. The buildings feature intersected with the fishnet feature; therefore, the buildings not only inside one single fishnet was divided to avoid the repeated calculations. The floor area of each fishnet was calculated using the spatial statistics method and converted to raster in ArcGIS.

2.2. LUOJIA 1-01 nighttime lights imagery

The satellite “LUOJIA 1-01” was launched at June. 2, 2018 and carries a nighttime light sensor with the 130-m spatial resolution. The

whole map of mainland China was combined with 275 images from June to December in 2018. The dataset was applied through the High resolution earth observation system to the Hubei data and application network (<http://www.hbeos.org.cn/>).

The LUOJIA 1-01 NTL image also suffers from the problem of saturation in urban areas, which was adjusted with the Vegetation Adjusted NTL Urban Index (VANUI). The detail of the VANUI method can be found in related literature (Zhang et al., 2013). Differences in the saturation reduction case studies that use NDVI derived from the moderate resolution imaging spectroradiometer (MODIS) (Ma et al., 2014) and the annual mean NDVI from Landsat in 2018 were used to reduce saturation and increase the variation in the LUOJIA 1-01 images, which was calculated with google earth engine platform.

2.3. Population mainland China dataset

The 100-m spatial resolution population dataset from 2017 was chosen as an independent variable, which was estimated based on the point of interest (POI), DMSP/OLS nighttime lights imagery, NDVI, DEM, Road, Census population data, and World population data (Ye et al., 2019). The census population data are typically reported at administrative unit levels, which is not suitable for the spatial analyses in this study. Hong Kong, Macao, and Taiwan were excluded from population dataset in 2017. Therefore, the predicted floor area (PFA) map did not include these three regions.

2.4. Chinese urban area map

Many global or regional urban land cover products have been generated. The built-up area in the global land use map (Gong et al., 2019) and the impervious surface map (Ma et al., 2014) are composed of road and building areas. This study does not consider roads. Although a map of 45 global cities with more detailed information about built-up

areas has been published (Shao et al., 2019), the dataset did not cover the entire study area. The dataset, which has a spatial resolution of 30 m, and is the newest global urban map produced based on Landsat images and the Google earth engine platform (Liu et al., 2018), is more suitable for this study.

3. Method

The building data processing, the floor area mapping with the RF model, and assessing accuracy is exhibited in Fig. 2.

3.1. Spatial resolution match

The spatial resolution in this study was aggregated to 130 m to match the LUOJIA 1-01 nighttime images. The population map was also resampled to 130 m spatial resolution. The calculated floor area (CFA) maps generated with single buildings for 71 cities were counted with a 130 m fishnet cell and converted to a raster map. All the raster and feature data were projected in the Albers Conical Equal Area projection.

3.2. Fitting the RF model and floor area mapping

The RF regression model was chosen to estimate the PFA map (response) using the LUOJIA 1-01 imagery and population map (predictors). The RF regression model is a widely used machine learning method that was generated from traditional tree-based methods (Breiman, 2001; Pfugmacher et al., 2014; Yoo et al., 2019) and is a non-parametric method that does not require tree pruning and independent estimates (Hastie et al., 2009). The calculation details and formulas of the RF method can be found in literature (Breiman, 2001).

The normalized LUOJIA 1-01 images and population maps were set as predictors to fit the RF model. The data for fitting the RF model were generated using a sample tool based on the LUOJIA 1-01 nighttime images; the population maps and CFA maps from the 50 of 71 cities were used as training samples. The PFA map was estimated with a calibrated RF model for all of mainland China. The urban area map (Liu et al., 2018) was used as a mask to define the boundary of the PFA map.

3.3. Accuracy assessment

The CFA maps of the other 21 cities were used to assess the total PFA map accuracy. A random 1% of the total cells in the 21 cities were derived from calculated and PFA maps to test the accuracy. Beijing, Qingdao, Shanghai, Chengdu, Guangzhou, and Harbin of 21 cities were selected to test the accuracy of single cities.

Two statistical measurements were used to assess the accuracy of the PFA map with significant correlation ($P < 0.005$) coefficient of determination (R^2 , Eq. (1)) and root mean square error (RMSE, Eq. (2)), as follows:

$$R^2 = 1 - \frac{(n-1)\sum_{i=1}^n (\hat{y}_i - y_i)^2}{(n-2)\sum_{i=1}^n (\hat{y}_i - \bar{y})^2} \quad (1)$$

$$RMSE = \sqrt{\frac{\sum_{i=1}^n (\hat{y}_i - y_i)^2}{n}} \quad (2)$$

where n is the number of samples, \hat{y}_i is the predicted FA value, and y_i is the CFA value.

3.4. FPFA map of China

To further improve the accuracy, the PFA map of mainland China was overlapped by CFA maps in 71 cities in corresponding locations; therefore, the final predicted floor area (FPFA) map of mainland China in 2017 was produced.

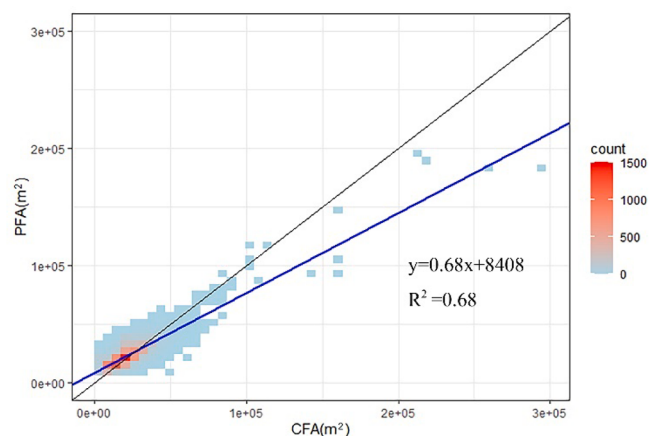


Fig. 3. Scatterplot of the CFA and PFA maps.

4. Results

4.1. Accuracy assessment of the PFA map

Fig. 3 shows that the total accuracy of the PFA map was strong ($R^2 = 0.68$, RMSE = 7277.46). The PFA map overestimated the values in low value areas and underestimated the values in high value areas.

Beijing, Qingdao, Shanghai, Chengdu, Guangzhou and Harbin, distributing in different geographic location of China, were selected to test the accuracy at the scale of a single city, considering its spatial location in China mainland. The building feature maps did not cover all the regions of urban area; therefore, the range of the CFA maps was smaller than that of the PFA map (Fig. 4). The accuracies of the PFA relative to those of the CFA maps increased in Beijing, Shanghai, Chengdu, Guangzhou, Qingdao and Harbin, and their R^2 's (slope coefficients) were 0.76 (0.72), 0.74 (0.76), 0.73 (0.75), 0.63 (0.68), 0.61, and 0.62 (0.59), which showed the accuracy in single city scale was acceptable. As the Fig. 3 shown, the regression line crossed the standard line at value 26275. Below the cross point, more point distributed upside area of the standard line, which means overestimations in the low value regions. Meanwhile, most part of the points over 80,000 located under the standard line area, which means few very high value regions exist in the CFA maps, which caused underestimations in the highly value regions.

4.2. FPFA map of mainland China in 2017

The CFA map of 71 cities was merged with the PFA map to replace the values with the corresponding location to generate the FPFA map of mainland China in 2017 (Fig. 5). Therefore, the FPFA map covered all the cities in mainland China. The total floor area is 76038.39 km², which represents 0.79% of total area of China. The area of CFA in the 71 cities was 16133.99 km², which represents 20.97% of total FPFA map with an area of 76954.40 km². The floor area of each pixel of the PFA map ranged from 420 to 227930 m²; however, the FPFA map ranged from 220 to 838225 m². Areas over 227930 m² only represents 0.21% and areas below 420 m² represent 3.45% of the total area.

The Floor area ratio (FAR) indicates the ratio of the floor area amount and the land area, which is an important index that reflects the real estate at the intensity development level (Liu et al., 2017). Higher values of FAR results in more density of buildings and high buildings. According to the Chinese construction standards, the value of FAR < 1, 1–2, 2–3, and > 3 indicates a low building intensity area, a multi-story buildings area, a high and mixed multi-story buildings area, and a high buildings area, with values of 50.98%, 44.06%, 4.54% and 0.42%, respectively. The area of FAR over 3 mainly locates in metropolitans; however, the area with a FAR value below 1 is mainly located in a

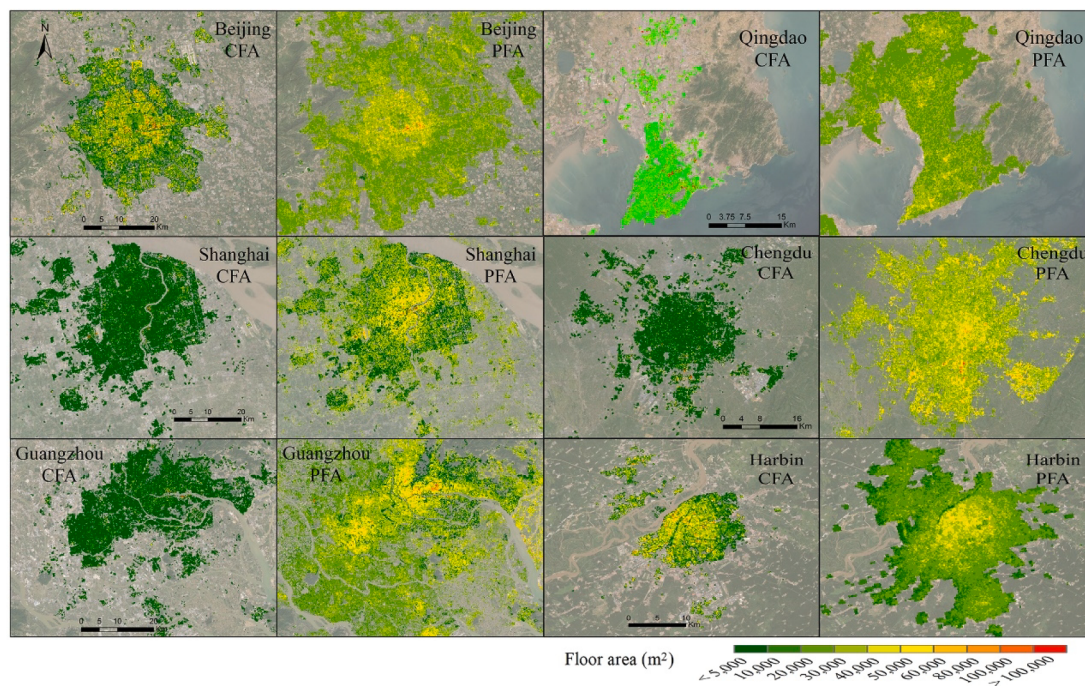


Fig. 4. Comparison of PFA and CFA maps for Beijing, Shanghai, Guangzhou, Qingdao, Chengdu, and Harbin.

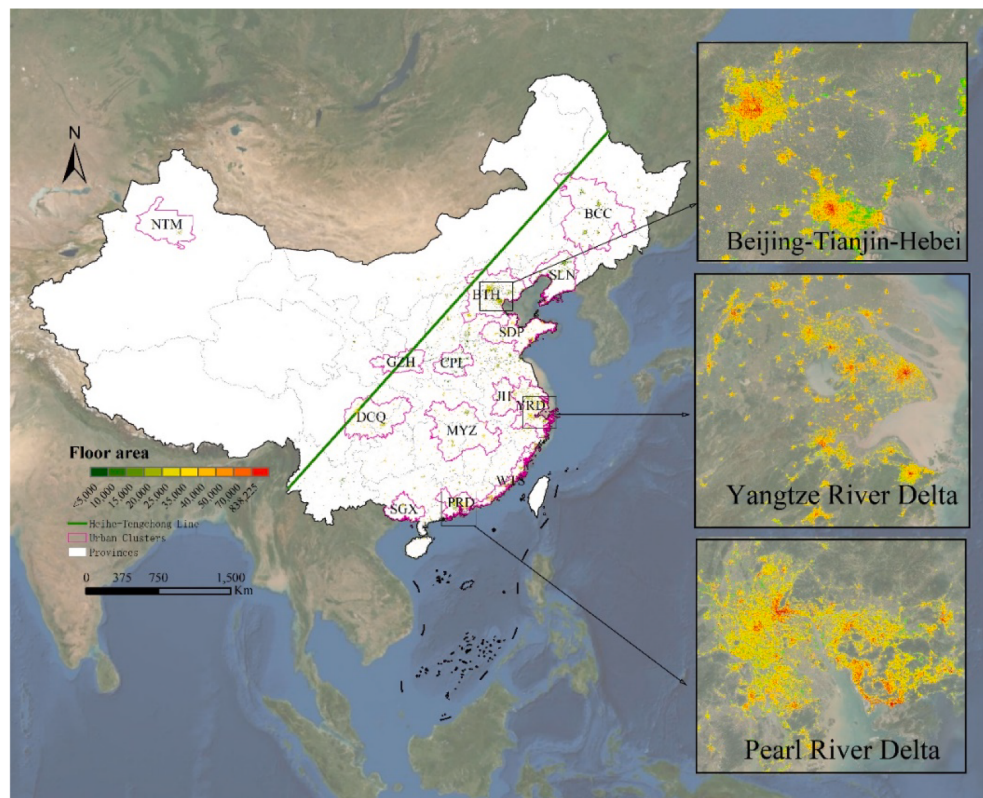


Fig. 5. Final floor area map of China's mainland.

suburb or little counties.

4.3. Spatial distribution of the PFA map

A total 98.23% of the floor area is located to the east of the Heihe-Tengchong line, a region which contains 43.8% of the land area and

94.1% of population of China (Fig. 5). The floor area and density of 14 of China's major UAs, proposed by Fang (Fang, 2015), were counted (Fig. 6). The total floor area of the 14 UAs was 66610.52 km², which was 70.59% of the total PFA. The Yangtze River Delta (YRD), Beijing-Tianjin-Hebei (BTH), Shandong Peninsula (SDP), Western Taiwan Straits (WTS) and Middle Yangtze (MYZ) are the five regions with the

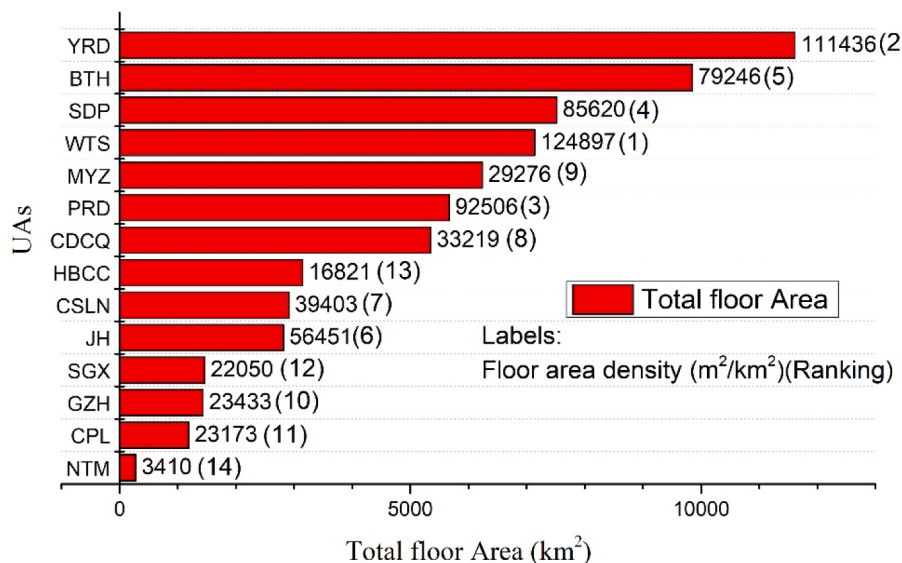


Fig. 6. Total floor area and density in 14 urban agglomerations in China. UAs: Urban agglomerations; YRD: Yangtze River Delta; BTH: Beijing-Tianjin-Hebei; SDP: Shandong Peninsula; WTS: Western Taiwan Straits; MYZ: Middle Yangtze; PRD: Pearl River Delta, CDCQ: Chengdu-Chongqing; HBCC: Harbin-Changchun, CSLN: Central and Southern Liaoning; JH: Jianghuai; SGX: Southern Guangxi; GZH: Guanzhong, CPL: Central Plains; and NTM: Northern Tianshan Mountains.

Table 2
Total floor area and intensity in provinces of China (km²).

Name	Total floor area	Ranking	Floor area intensity	Ranking
Shandong	10037.65	1	68269.94	5
Guangdong	9964.59	2	52229.29	7
Jiangsu	8380.17	3	84789.59	4
Zhejiang	7005.58	4	68148.52	6
Hebei	6372.88	5	36232.93	9
Fujian	5430.01	6	42867.32	8
Anhui	4214.69	7	30508.46	10
Sichuan	4028.27	8	8327.84	22
Jiangxi	3673.85	9	21467.01	13
Liaoning	3428.26	10	25200.38	11
Guangxi	3361.21	11	13306.89	18
Henan	3122.80	12	19457.81	14
Hubei	3015.99	13	16356.55	15
Hunan	2804.34	14	12910.35	19
Beijing	2612.02	15	170091.73	3
Tianjin	2385.55	16	220072.84	1
Shanxi	2179.81	17	14685.32	17
Jilin	1852.00	18	10460.57	20
Chongqing	1837.66	19	22299.80	12
Shaanxi	1733.41	20	8767.50	21
Heilongjiang	1600.81	21	3819.74	24
Shanghai	1135.83	22	183043.37	2
Guizhou	1068.96	23	5880.46	23
Inner Mongolia	881.42	24	827.27	28
Hainan	703.54	25	14797.49	16
Yunnan	700.65	26	1732.31	26
Gansu	365.34	27	906.51	27
Xinjiang	309.34	28	202.76	29
Ningxia	112.58	29	2283.35	25
Qinghai	42.04	30	62.97	30
Tibet	2.31	31	1.95	31

greatest floor areas, which was consistent with the population amount. However, the WTS, YRD, Pearl River Delta (PRD), SDP and BTH are the five top regions with the highest floor area intensities and are located on the coastline of China. Fig. 6 shows that the inland floor area intensity UAs values were lower than those of the UAs along the coastline and are decreasing from south to north along the coastline due to economic development and topographic limit.

The statistics for the floor area and intensity of 31 provinces and municipalities demonstrated that Shandong, Guangdong, Jiangsu,

Zhejiang, Hebei, and Fujian were the six provinces with the highest floor area values (Table 2), which are all located on the east coastline. Tianjin, Shanghai and Beijing were the three provinces with the highest floor area intensities and are all municipalities with more built-up area. Jiangsu, Shandong, Zhejiang, Guangdong, Fujian and Hebei were the top six provinces with the highest floor area intensity values and are, except Hebei province, also located on the east coastline. The length of the coastlines of the top six provinces are Guangdong, Fujian, Shandong, Zhejiang, Liaoning and Hainan, and top six GDT values came from Guangdong, Jiangsu, Shandong, Zhejiang, Henan, and Sichuan provinces in 2017, which did not show same trend with the floor area amount and intensity. The spatial distribution of the floor area was mainly decided by the economic level and geographic conditions. The floor area in the last eight provinces was 3117.23 km², which was only 3.30% of the total floor area in mainland China, and 31.06% of the Shandong province. Qinghai and Tibet provinces have had the lowest floor area and intensity values.

5. Discussion

5.1. Prediction factors choose

Several factors, other than LUOJIA 1-01 images and population maps, were chosen to estimate the FA maps in a preliminary study, including points of interest (POIs), roads, slope, elevation, and normalized difference vegetation index (NDVI) data. The POI data include bank, hotel, park, restaurant, factory, and gas station information, which was used to generate a POI density map. The road features data were converted to a road density map. Different combinations of factors were tested; the results showed that the accuracy of the population map and the LUOJIA 1-01 images was the highest. The NDVI reflects the vegetation conditions, which were used to generate the land use conditions, the amount of urban impervious surfaces, and the generation of built-up area maps (Gong et al., 2019; Ma et al., 2014). However, the dependent variable is the floor area value, which is not only the land use category but also part of the area; therefore, the NDVI is not relevant and is uncertain. The same is true for the topographical factors, elevation, and slope, which are meaningful for identifying land use categories, but contribute less to floor area calculations. The accuracy of the POI density, population map, and LUOJIA 1-01 images is lower than those generated when the last two characteristics are

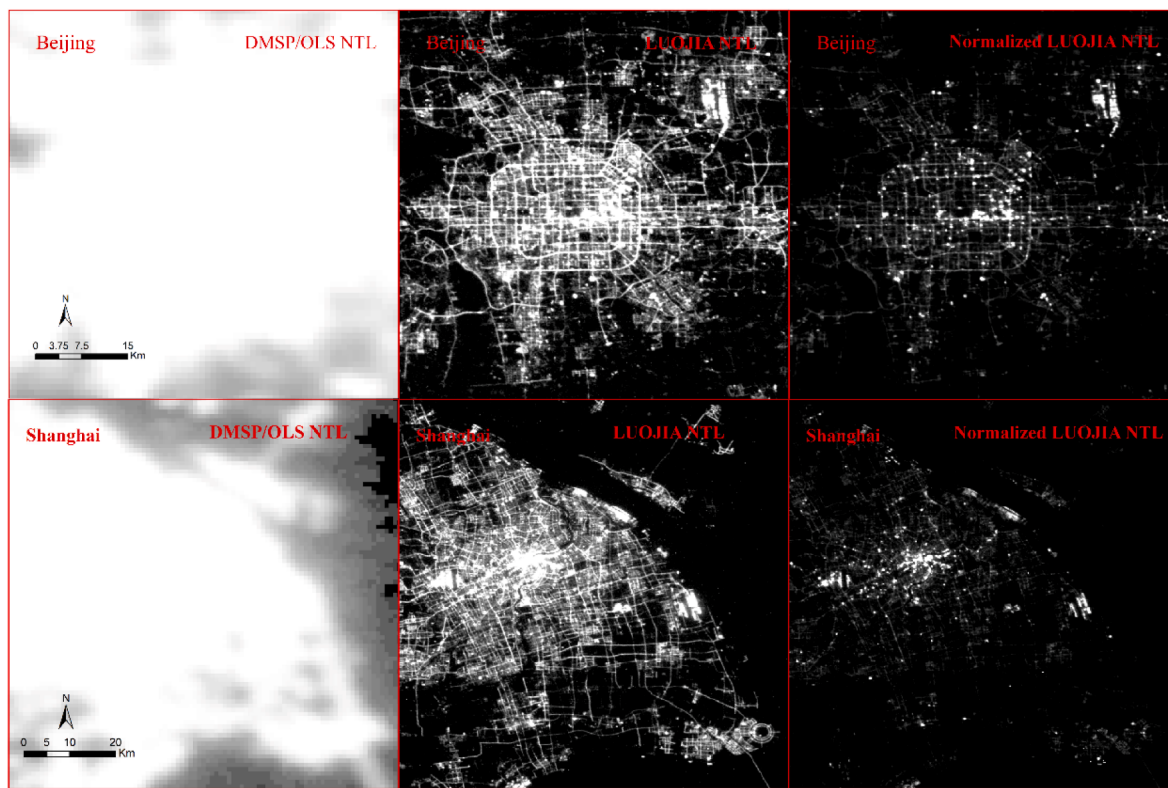


Fig. 7. Comparison between DMSP/OLS, LUOJIA 1-01 and normalized LUOJIA 1-01 NTL images.

combined, which may explain why the POI density map is highly correlated with the population map and different POIs have different relevance with floor area. Therefore, although only two factors were included in the estimation process, it produced the best results.

5.2. Implication of the PFA map

Many case studies have focused on how the three-dimensional patterns describe and eco-environmental process, which is an important topic in landscape ecology and urban ecology (Huang and Wang, 2019; Tian et al., 2019). Single buildings feature dataset is the most precise and ideal data for urban 3-dimensional studies (Liu et al., 2017). However, most of the study cases were studied at the district or city scale due to the difficulty of obtaining data at a large scale. The FA map of China can provide a valid dataset for spatial pattern analysis in different climatic zones and topographic conditions. The FA map will support research on the relationship between the 3-D pattern and eco-environmental processes at a national scale. In air pollution and heat island studies, the urban area and built-up areas were one important factor (Huang and Wang, 2019). In large scale studies, the urban area information was treated as one of the land use categories. Only in small scale studies was the 3-D information considered in spatial analyses or model prediction. The FA map provides a new whole buildings construction framework for all cities in China, which is meaningful for the analysis at the national and urban agglomeration and city scales. The FA map is also useful for ecological service and habitat estimation of urban garden (He et al.), buildings' green visibility (Yu et al., 2016), urban biodiversity (Lambert and Donihue, 2020) and urban heat island and health risk (Manoli et al., 2019) etc.

Expect eco-environmental studies, the FA is potentially useful for many other socio-economic studies, such as CO₂ emissions (Wang et al., 2019), CO₂ stock and absorption (Xie et al., 2016), material stock flows in built environment and urban infrastructure (Han et al., 2018; Schiller et al., 2020), and other socio-economic activities. Urbanization is not

only the expansion of built-up area, but also the increase of building heights caused by old city reconstruction and urban renewal (He et al., 2017). The FA map could provide great support for urban governor to carry out comprehensive planning and management of urban horizontal and vertical development. In the past, urban planning and management only focused on the growth of urban area, but did not pay enough attention to the increase of internal building height.

5.3. Comparing LUOJIA 1-01 imagery with other NTL sources of data

There are numerous available NTL sensors (Levin et al., 2020), of which the DMSP/OLS and VIIRS/DNB images were widely used as NTL sources of data for regional and global research, which can provide important data for extracting information about land surface classification and change, such as at the urban expansion, impervious surface, built-up area, urban agglomeration spatial development at global, continental, and national scales (Elvidge et al., 1999; Miller et al., 2012; Peng et al., 2020). The spatial resolutions of DMSP/OLS and VIIRS/DNB images are 3000 and 740 m, which are not enough to reflect the urban inside information. The Landsat 8 could be treated as TNL images with a high spatial resolution of 30 m, but only a very few bright objects can be detected in the images (Levin and Phinn, 2016). The NTL images or pictures from the International Space Station are also available at a high spatial resolution (5–200 m); however, the irregularly archive data causes the difficulty of application (Sánchez de Miguel et al., 2019).

Compared with widely used DMSP/OLS and VIIRS/DNB images, the spatial resolution of the LUOJIA 1-01 images improved to 130 m, which allows the possibility that the urban inside detail information will be reflected (Li et al., 2018; Liu et al., 2012). The NTL images suffer from the problem of saturation in an urban area. The comparison of the images of DMSP/OLS with the original and adjusted LUOJIA 1-01 with VANUI images in Beijing and Shanghai cities demonstrated the quality of LUOJIA 1-01 images (Fig. 7). The range of the Digital Number (DN) values in DMSP/OLS, LUOJIA 1-01, and the normalized LUOJIA 1-01

images are 1-63, 1-423806 and 1-15040700, respectively. The spatial resolution and DN improvement would cause the LUOJIA 1-01 images to reflect much more detailed information. Combined with POIs, statistical or observed data, characters of the urban inside region or human-activities can be reflected, such as the traffic situation, electric consumption, buildings lodging ratio; night-time heat island, etc. At present, only data from mainland China is available from the LUOJIA satellite sensors. With the archive data increasing, more temp-spatial scale and time-series studies can be carried out in future.

6. Conclusion

In this study, we attempted to product the first urban floor area map in national scale with new high spatial resolution NTL image and big data method for developing urban morphology and expansion analysis in 3-dimensional scale, which is essential for urban ecology and planning study, such as urban heat island, air pollution effect, road system and urban green space design and so on. The mainland China floor area map was estimated with LUOJIA 1-01 NTL images, population maps and a single building dataset for 71 cities within an RF model at a 130-m spatial resolution in 2017. The total accuracy of the map was acceptable was strong ($R^2 = 0.68$, RMSE = 7277.46). A total of 98.23% of the floor area was located east of the Heihe-Tengchong line, and the east coastline was the highest intensity area, especially in several main urban agglomerations.

The potential implication of the map in eco-environmental and socio-economic studies were discussed. Comparing with present available NTL sources of data, the LUOJIA 1-01 images have the most high spatial resolution for determining urban inside information at a large spatial scale.

One limitation of our study was that the map underestimated the floor area in the high value regions and overestimation in low value regions, which would cause the uncertainty in small scale study. So, the mainland China floor area map is suitable for implication in large scale, not suitable for the studies in single city scale. With the LUOJIA 1-01 images archived data accumulation, a global floor area map could be produced in near future. Meanwhile, relationship of the eco-environmental and socio-economic process and urban 3-D morphology could be carried out with our map in large scale.

Declaration of Competing Interest

The authors declare that they have no known competing financial interests or personal relationships that could have appeared to influence the work reported in this paper.

Acknowledgements

This research was financially supported by the National Natural Science Foundation of China (No. 32071580, 41730647 and 41871192), the Youth Innovation Promotion Association of CAS (2021194).

References

- Alavipanah, S., Schreyer, J., Haase, D., Lakes, T., & Qureshi, S. (2018). The effect of multi-dimensional indicators on urban thermal conditions. *Journal of Cleaner Production*, 177, 115–123.
- Amaral, S., Câmara, G., Monteiro, A. M. V., Quintanilha, J. A., & Elvidge, C. D. (2005). Estimating population and energy consumption in Brazilian Amazonia using DMSP night-time satellite data. *Computers, Environment and Urban Systems*, 29(2), 179–195.
- Breiman, L. J. M. L. (2001). *Random Forests*, 45(1), 5–32.
- Cao, Q., Luan, Q., Liu, Y., & Wang, R. (2021). The effects of 2D and 3D building morphology on urban environments: A multi-scale analysis in the Beijing metropolitan region. *Building and Environment*, 192, Article 107635.
- Doll, C. H., Muller, J.-P., & Elvidge, C. D. (2000). Night-time imagery as a tool for global mapping of socioeconomic parameters and greenhouse gas emissions. *AMBO: A Journal of the Human Environment*, 29(3), 157–162.
- Elvidge, C. D., Baugh, K. E., Dietz, J. B., Bland, T., Sutton, P. C., & Kroehl, H. W. (1999). Radiance calibration of DMSP-OLS low-light imaging data of human settlements. *Remote Sensing of Environment*, 68(1), 77–88.
- Fang, C. (2015). Important progress and future direction of studies on China's urban agglomerations. *Journal of Geographical Sciences*, 25(8), 1003–1024.
- Flörke, M., Schneider, C., & McDonald, R. I. (2018). Water competition between cities and agriculture driven by climate change and urban growth. *Nature Sustainability*, 1(1), 51–58.
- Ge, Y., Hu, S., Ren, Z., Jia, Y., Wang, J., Liu, M., et al. (2019). Mapping annual land use changes in China's poverty-stricken areas from 2013 to 2018. *Remote Sensing of Environment*, 232, Article 111285.
- Gong, P., Liu, H., Zhang, M., Li, C., Wang, J., Huang, H., et al. (2019). Stable classification with limited sample: Transferring a 30-m resolution sample set collected in 2015 to mapping 10-m resolution global land cover in 2017. *Science Bulletin*, 64(6), 370–373.
- Gong, P., Wang, J., Yu, L., Zhao, Y., Liang, L., et al. (2013). Finer resolution observation and monitoring of global land cover: First mapping results with Landsat TM and ETM+ data. *International Journal of Remote Sensing*, 34(7), 2607–2654.
- Han, J., Chen, W.-Q., Zhang, L., & Liu, G. (2018). Uncovering the spatiotemporal dynamics of urban infrastructure development: A high spatial resolution material stock and flow analysis. *Environmental Science & Technology*, 52(21), 12122–12132.
- He, C., Liu, Z., Tian, J., Ma, Q. J. G. C. B., Urban expansion dynamics and natural habitat loss in China: A multiscale landscape perspective, 20(9):2886–2902.
- He, Q., Liu, Y., Zeng, C., Chaohui, Y., & Tan, R. (2017). Simultaneously simulate vertical and horizontal expansions of a future urban landscape: A case study in Wuhan, Central China. *International Journal of Geographical Information Science*, 31(10), 1907–1928.
- Hu, X., Qian, Y., Pickett, S. T. A., & Zhou, W. (2020). Urban mapping needs up-to-date approaches to provide diverse perspectives of current urbanization: A novel attempt to map urban areas with nighttime light data. *Landscape and Urban Planning*, 195, Article 103709.
- Huang, X., & Wang, Y. (2019). Investigating the effects of 3D urban morphology on the surface urban heat island effect in urban functional zones by using high-resolution remote sensing data: A case study of Wuhan, Central China. *ISPRS Journal of Photogrammetry and Remote Sensing*, 152, 119–131.
- Kedron, P., Zhao, Y., & Frazier, A. E. (2019). Three dimensional (3D) spatial metrics for objects. *Landscape Ecology*, 34(9), 2123–2132.
- Khosravi, I., Momeni, M., & Rahnamoonfar, M. (2014). Performance evaluation of object-based and pixel-based building detection algorithms from very high spatial resolution imagery. *Photogrammetric Engineering and Remote Sensing*, 80(6), 519–528.
- LImhoff, M., Lawrence, W. T., Stutzer, D. C., Elvidge, C. D., 1997, A technique for using composite DMSP/OLS "City Lights" satellite data to map urban area, *Remote Sensing of Environment* 61(3):361-370.
- Lambert, M. R., & Donihue, C. M. (2020). Urban biodiversity management using evolutionary tools. *Nature Ecology & Evolution*.
- Leinenkugel, P., Esch, T., & Kuenzer, C. (2011). Settlement detection and impervious surface estimation in the Mekong Delta using optical and SAR remote sensing data. *Remote Sensing of Environment*, 115(12), 3007–3019.
- Levin, N., Kyba, C. C. M., Zhang, Q., Sánchez de Miguel, A., Román, M. O., Li, X., et al. (2020). Remote sensing of night lights: A review and an outlook for the future. *Remote Sensing of Environment*, 237, Article 111443.
- Levin, N., & Phinn, S. (2016). Illuminating the capabilities of Landsat 8 for mapping night lights. *Remote Sensing of Environment*, 182, 27–38.
- Li, M., Koks, E., Taubenböck, H., & van Vliet, J. (2020). Continental-scale mapping and analysis of 3D building structure. *Remote Sensing of Environment*, 245, Article 111859.
- Li, S., Cheng, L., Liu, X., Mao, J., Wu, J., & Li, M. (2019). City type-oriented modeling electric power consumption in China using NPP-VIIRS nighttime stable light data. *Energy*, 189, Article 116040.
- Li, X., Zhao, L., Li, D., Xu, H., 2018, Mapping Urban Extent Using Luojia 1-01 Nighttime Light Imagery, 18(1):3665.
- Li, X. C., & Zhou, Y. Y. (2017). Urban mapping using DMSP/OLS stable night-time light: A review. *International Journal of Remote Sensing*, 38(21), 6030–6046.
- Liu, D., Chen, N., Zhang, X., Wang, C., & Du, W. (2020). Annual large-scale urban land mapping based on Landsat time series in Google Earth Engine and OpenStreetMap data: A case study in the middle Yangtze River basin. *ISPRS Journal of Photogrammetry and Remote Sensing*, 159, 337–351.
- Liu, M., Hu, Y.-M., & Li, C.-L. (2017). Landscape metrics for three-dimensional urban building pattern recognition. *Applied Geography*, 87, 66–72.
- Liu, X., Hu, G., Ai, B., Li, X., & Shi, Q. (2015). A Normalized Urban Areas Composite Index (NUACI) based on combination of DMSP-OLS and MODIS for mapping impervious surface area. *Remote Sensing*, 7(12), 17168–17189.
- Liu, X., Hu, G., Chen, Y., Li, X., Xu, X., Li, S., ... Wang, S. (2018). High-resolution multi-temporal mapping of global urban land using Landsat images based on the Google Earth Engine Platform. *Remote Sensing of Environment*, 209, 227–239.
- Liu, Z., He, C., Zhang, Q., Huang, Q., & Yang, Y. (2012). Extracting the dynamics of urban expansion in China using DMSP-OLS nighttime light data from 1992 to 2008. *Landscape and Urban Planning*, 106(1), 62–72.
- Lo, C. P. (2001). Modeling the population of China using DMSP operational linescan system nighttime data. *Photogrammetric Engineering and Remote Sensing*, 67, 1037–1047.
- Ma, Q., He, C., Wu, J., Liu, Z., Zhang, Q., & Sun, Z. (2014). Quantifying spatiotemporal patterns of urban impervious surfaces in China: An improved assessment using nighttime light data. *Landscape and Urban Planning*, 130, 36–49.
- Ma, T., Zhou, C., Pei, T., Haynie, S., & Fan, J. (2012). Quantitative estimation of urbanization dynamics using time series of DMSP/OLS nighttime light data: A

- comparative case study from China's cities. *Remote Sensing of Environment*, 124, 99–107.
- Manoli, G., Faticchi, S., Schläpfer, M., Yu, K., Crowther, T. W., Meili, N., et al. (2019). Magnitude of urban heat islands largely explained by climate and population. *Nature*, 573(7772), 55–60.
- Miller, S. D., Mills, S. P., Elvidge, C. D., Lindsey, D. T., Lee, T. F., Hawkins, J. D., 2012, Suomi satellite brings to light a unique frontier of nighttime environmental sensing capabilities, 109(39):15706-15711.
- Niemeyer, J., Rottensteiner, F., & Soergel, U. (2014). Contextual classification of lidar data and building object detection in urban areas. *ISPRS Journal of Photogrammetry and Remote Sensing*, 87, 152–165.
- Ok, A. O. (2013). Automated detection of buildings from single VHR multispectral images using shadow information and graph cuts. *Isprs Journal of Photogrammetry and Remote Sensing*, 86, 21–40.
- Peng, J., Lin, H., Chen, Y., Blaschke, T., Luo, L., Xu, Z., Hu, Y. n., Zhao, M., Wu, J., 2020, Spatiotemporal evolution of urban agglomerations in China during 2000–2012: a nighttime light approach, *Landscape Ecology*.
- Pflugmacher, D., Cohen, W. B., Kennedy, R. E., & Yang, Z. (2014). Using Landsat-derived disturbance and recovery history and lidar to map forest biomass dynamics. *Remote Sensing of Environment*, 151, 124–137.
- Sánchez de Miguel, A., Kyba, C. C. M., Aubé, M., Zamorano, J., Cardiel, N., Tapia, C., et al. (2019). Colour remote sensing of the impact of artificial light at night (I): The potential of the International Space Station and other DSLR-based platforms. *Remote Sensing of Environment*, 224, 92–103.
- Sawaya, K. E., Olmanson, L. G., Heinert, N. J., Brezonik, P. L., & Bauer, M. E. (2003). Extending satellite remote sensing to local scales: Land and water resource monitoring using high-resolution imagery. *Remote Sensing of Environment*, 88(1), 144–156.
- Schiller, G., Bimesmeier, T., Pham, A. T. V., 2020, Method for Quantifying Supply and Demand of Construction Minerals in Urban Regions—A Case Study of Hanoi and Its Hinterland, 12(11):4358.
- Schunert, A., & Soergel, U. (2012). Grouping of Persistent Scatterers in high-resolution SAR data of urban scenes. *ISPRS Journal of Photogrammetry and Remote Sensing*, 73, 80–88.
- Seto, K. C., Kaufmann, R. K., & Woodcock, C. E. J. N. (2000). Landsat reveals China's farmland reserves, but they're vanishing fast. *Nature*, 406(6792), 121.
- Shao, Z., Fu, H., Li, D., Altan, O., & Cheng, T. (2019). Remote sensing monitoring of multi-scale watersheds impermeability for urban hydrological evaluation. *Remote Sensing of Environment*, 232, Article 111338.
- Statistics, C. n. b. o., 2018, China city statistical yearbook, Chinese statistics press.
- Suveg, I., Vosselman, G., 2002, Automatic 3D building reconstruction, pp. 59–69.
- Tian, Y., Zhou, W., Qian, Y., Zheng, Z., & Yan, J. (2019). The effect of urban 2D and 3D morphology on air temperature in residential neighborhoods. *Landscape Ecology*, 34 (5), 1161–1178.
- UN, 2018, World urbanization prospects, 2018 revision, New York: United Nations.
- Wang, H., Liu, G., & Shi, K. (2019). What are the driving forces of urban CO₂ emissions in China? A refined scale analysis between national and urban agglomeration levels. *International Journal of Environmental Research and Public Health*, 16(19), 3692.
- Xi, F., Davis, S. J., Ciais, P., Crawfordbrown, D., Guan, D., Pade, C., Shi, T., Syddall, M., Lv, J., Ji, L., 2016, Substantial global carbon uptake by cement carbonation, (12).
- Xu, Y. Y., Liu, M., Hu, Y. M., Li, C. L., & Xiong, Z. P. (2019). Analysis of three-dimensional space expansion characteristics in old industrial area renewal using GIS and Barista: A case study of Tiexi District, Shenyang, China. *Sustainability*, 11(7).
- Ye, T., Zhao, N., Yang, X., Ouyang, Z., Liu, X., Chen, Q., et al. (2019). Improved population mapping for China using remotely sensed and points-of-interest data within a random forests model. *Science of The Total Environment*, 658, 936–946.
- Yoo, C., Han, D., Im, J., & Bechtel, B. (2019). Comparison between convolutional neural networks and random forest for local climate zone classification in mega urban areas using Landsat images. *ISPRS Journal of Photogrammetry and Remote Sensing*, 157, 155–170.
- Yu, S., Yu, B., Song, W., Wu, B., Zhou, J., Huang, Y., et al. (2016). View-based greenery: A three-dimensional assessment of city buildings' green visibility using Floor Green View Index. *Landscape and Urban Planning*, 152, 13–26.
- Zhang, Q., Schaaf, C., & Seto, K. C. (2013). The Vegetation Adjusted NTL Urban Index: A new approach to reduce saturation and increase variation in nighttime luminosity. *Remote Sensing of Environment*, 129, 32–41.
- Zhang, Q., & Seto, K. C. (2011). Mapping urbanization dynamics at regional and global scales using multi-temporal DMSP/OLS nighttime light data. *Remote Sensing of Environment*, 115(9), 2320–2329.
- Zhao, C., Weng, Q., & Hersperger, A. M. (2020). Characterizing the 3-D urban morphology transformation to understand urban-form dynamics: A case study of Austin, Texas, USA. *Landscape and Urban Planning*, 203, Article 103881.
- Zheng, Z., Zhou, W., Yan, J., Qian, Y., Wang, J., & Li, W. (2019). The higher, the cooler? Effects of building height on land surface temperatures in residential areas of Beijing. *Physics and Chemistry of the Earth, Parts A/B/C*, 110, 149–156.